

MONTE-CARLO MODELING OF SILICON X-RAY DETECTORS

Brian Cross⁽¹⁾, Greg Bale⁽²⁾, Barrie Lowe⁽²⁾ and Rob Sareen⁽²⁾

(1) *CrossRoads Scientific, 414 Av. Portola, El Granada, CA 94018-1823, USA.*

(2) *Gresham Scientific Instruments, Ltd., Sirius House, Watery Lane, Wooburn Green, Buckinghamshire, HP10 0AP, UK.*

ABSTRACT

A new 3-D Monte-Carlo code, X-Tracker, was developed to model internal events that occur as X-ray photons are absorbed within Si(Li) detectors. The goal was to model the performance of state-of-the-art detectors, including peak shapes, background and “artifact” peaks found in “clean spectra” from collimated radioactive and other X-ray sources. The model includes the influence of collimation, front contacts, crystal traps or “defects,” passivation walls, dead layers and other boundary effects. Photon fluorescence and scatter and electron effects (including Auger, Photo and Compton electrons) have been included. Monte Carlo and analytical models have been blended to take advantage of both approaches, including the reflection-coefficient concept that explains how charge-carrier collection can be improved with suitable designs of the front interfacial layer. Good agreement has been demonstrated between simulated and real spectra, although there is still some room for improvement. The program has demonstrated its use as a tool for both understanding problems with earlier detector designs, and for improved designs where the need exists for detectors with very clean response functions, in applications such as synchrotron beam lines and polarized XRF spectrometers.

INTRODUCTION

Although there has been a growing body of Monte-Carlo programs used in X-ray spectrometry since the advent of fast low-cost personal computers, most have simulated the photon-sample interactions [e.g. 1-4], rather than detailed studies of the processes inside an X-ray detector. In this work, an analytical, and often empirical, detector response function is usually applied to the final signal into the detector. Recently, programs have been extended to model not only the photon but also the electron interactions in samples, such as Mantler [5] for multilayer thin-film analysis. There have been exceptions, of course, and recent work by Campbell [6] and Eggert [7] is especially noteworthy for modeling directly the silicon detector.

To completely model the interactions inside a detector we must include both photon and electron generation and scattering. Much work has been done on Monte-Carlo modeling of electron scattering, including Joy [8] and others [9, 10]. Other work relevant to modeling detectors includes that by Bale [11], who was concerned with modeling Cd-Zn-Te detectors used in space applications, which have very different characteristics to Si(Li) detectors. We were able to modify this work and adapt it to Si(Li) detectors, adding the necessary and unique features.

THEORY

There are many books describing the Monte-Carlo method and its application, including Joy [8] and a more general book by Kalos and Whitlock [12], which describes the general Monte-Carlo techniques. Initially, incoming X-ray photons, with an energy selected randomly from a probability distribution (a “line” spectrum), are given a random pair of angles and/or coordinates of entry into the detector. The entry area is defined by the detector collimator, which may be circular or square. The initial photon vector is then defined for a point source or a parallel beam, in polar or Cartesian coordinates respectively. Internally it is simpler to track events with polar

This document was presented at the Denver X-ray Conference (DXC) on Applications of X-ray Analysis.

Sponsored by the International Centre for Diffraction Data (ICDD).

This document is provided by ICDD in cooperation with the authors and presenters of the DXC for the express purpose of educating the scientific community.

All copyrights for the document are retained by ICDD.

Usage is restricted for the purposes of education and scientific research.

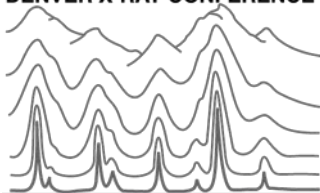
DXC Website

– www.dxcicdd.com

ICDD Website

- www.icdd.com

DENVER X-RAY CONFERENCE®



vectors, but these must be converted to a Cartesian geometry to check if the current position is inside the detector frame.

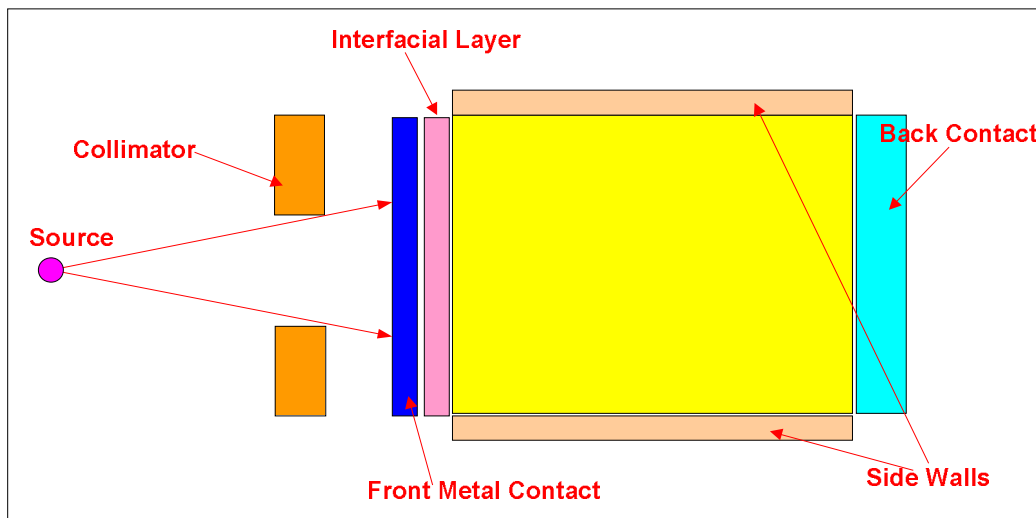


Figure 1. Cross-Section of an X-Ray Detector with X-Ray Source and Collimator.

Figure 1 shows a model of the main detector components, with front metal contact, interfacial (or “dead”) layer, active detector volume with a passivation layer on its side walls, and back contact. In addition the front collimator is shown with a point representing the source of incoming X-ray photons. X-Tracker models the detector as a right square prism although this may affect the accuracy of edge modeling in some cases, as many detectors have circular cross-sections. All other aspects of the experimental setup are fully modeled, such as the choice of point source or parallel beam, the cross-sectional areas of the detector and the collimator, the depths of the front and back contacts, the interfacial layer and the active volume.

The main steps in the Monte-Carlo model are:

- (a) Initialize and fill arrays (charge collection efficiency, etc.);
- (b) Define geometry and randomize starting position/vector coordinates;
- (c) Select photon energy from input source line spectrum file;
- (d) Call front electrode function, tracking photons and electrons;
- (e) Transfer electrons and photons from (d) and do same for dead layer, if present;
- (f) Transfer electrons and photons from (e) and do same for main active volume;
- (g) Consider and track all photon-silicon events based upon relative probabilities of photoelectric absorption, Compton and Rayleigh scatter;
- (h) Track all emitted electrons, calculate electron ranges, generate charge events;
- (i) Convolve charge with reflection effects, collection efficiencies, traps, statistical broadening;
- (j) Convert charge to energy and deposit in spectrum channel;
- (k) After simulation terminates, add zero strobe peak, and generate any passivation or back contact fluorescence events and add to spectrum, and display spectrum.

At the start of the simulation, an array of charge collection efficiency factors, at different depths from the detector front, is generated. When a photon is absorbed within an active detector

crystal, a charge cloud is generated at a given depth. The electrons and holes are separated by the applied electric field, and drift to their respective electrodes as illustrated in Figure.2.

Holes and electrons have different mobilities and lifetimes that depend upon temperature and resistivity. The lithium drifting process compensates the inherent impurities in a silicon crystal, improving the resistivity and carrier properties. The back of the detector is usually not compensated, resulting in an inactive n^+ region that may be quite large. For the active region, the assumption is made that the applied field is uniform across the active region, given by:

$$\xi = V/d \quad (1)$$

where V is the bias and d is the thickness. The electric field profile for a Si(Li) detector is shown in Figure 3, compared with that for a depleted detector such as high-purity Ge (HPGe).

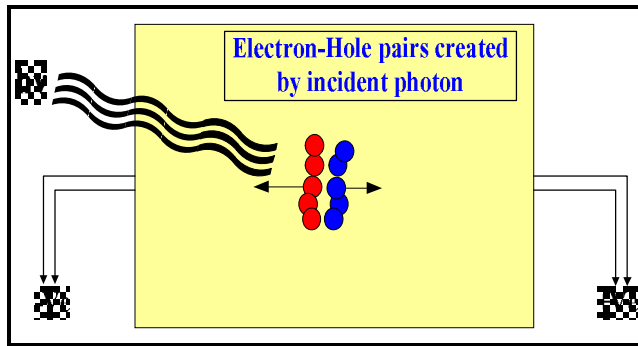


Figure 2. Electron-Hole Pair Creation

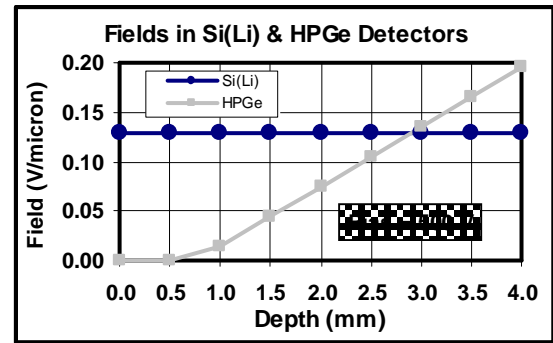


Figure 3. Electric Field in a Si(Li)

Detectors such as Si-pin diodes or high-purity intrinsic germanium crystals have fields that vary from the front to the rear. In a uniform field gradient, the relationship for induced charge from a motion dx of electrons (dx_e) and holes (dx_h) is given by the Shockley-Ramo Theorem [13-14]:

$$dQ^* = -(eN_0/L) * (dx_e + dx_h) \quad (2)$$

where dQ^* is the induced charge, N_0 is the initial number of electron-hole pairs, L is the detector depth, and e is the electronic charge. Unless the detector is defect free, significant charge trapping may occur at any depth, and the induced charge becomes a function of the distance over which the charge travels. The trapping probability depends on the density of the traps, which may be impurities or defects in the crystal including unpaired lithium ions. Often preferential hole traps dominate. Charge collection efficiency, in the case of a uniform electric field and trapping, is described by the Hecht equation [15] given in equation (3), as revised by Akutagawa and Zanio [16], where v is the carrier mobility, τ is the carrier lifetime, x_i is the interaction depth, L is the detector thickness and the e and h subscripts represent electrons and holes respectively.

$$Q^* = \frac{eN_0}{L} \cdot \left[v_h \tau_h \left(1 - \exp \left[\frac{-x_i}{v_h \tau_h} \right] \right) \right] + \left[v_e \tau_e \left(1 - \exp \left[\frac{x_i - L}{v_e \tau_e} \right] \right) \right] \quad (3)$$

Using default values for the electron and hole lifetimes and mobilities, the charge collection efficiency table calculated by X-Tracker, using equation (3), is shown in Figure 4. The efficiency as a function of detector depth is very flat and remains almost at 100%. The value only drops to about 98% after about 4 mm. A second table is also calculated that ignores the

transport of holes, and is used to model charge traps. This plot (also shown in Figure 4) is very different from that with both holes and electrons, demonstrating the importance of good hole mobility and full collection. Si(Li) detectors show excellent response over a wide energy range, having efficiently collected the holes.

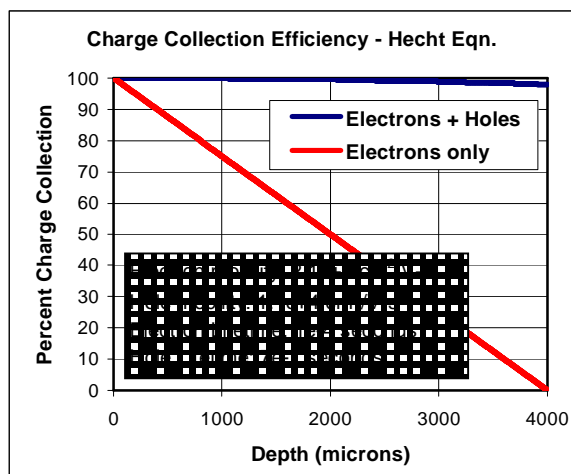


Figure 4. Charge Collection Efficiencies

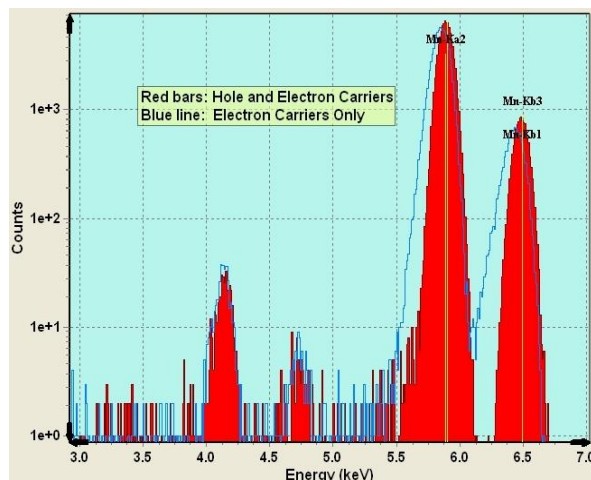


Figure 5. Effect of Carriers

Figure 5 compares two simulated Fe-55 spectra, calculated with the two Hecht efficiency tables from Figure 4. Now we include the charge reflection effect at the detector front surface [17-18].

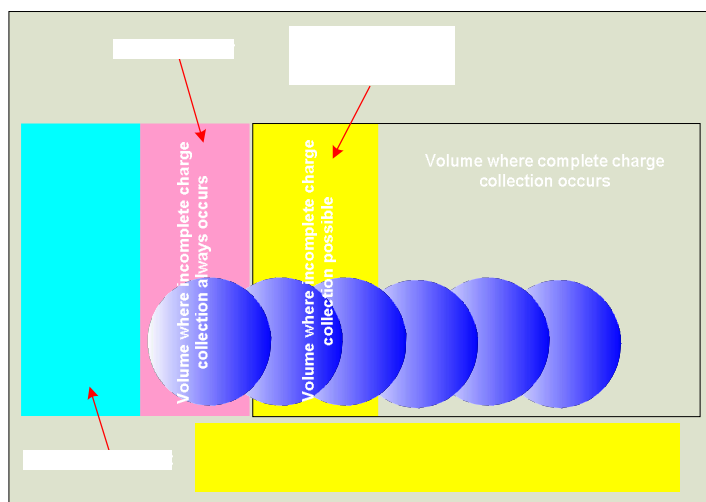


Figure 6. Charge Clouds near Front Surface.

Silicon detector metal contacts have been extensively researched (e.g. [19]). The Schottky front surface partially reflects the charge cloud, so more carriers are collected than would occur from simple geometry that assumes part of the charge cloud occurs in or drifts into a dead region. The interfacial layer, between the active region and the front contact, can be designed to enhance this reflection process. Figure 7 shows the effect of changing the Reflection Coefficient (RC). These are simulated spectra, where the hot electron losses and electrode effects were disabled to show the RC effects more clearly. When the RC is 0.9, there is virtually no tailing. When the RC is zero, the low energy cutoff in the background occurs at half the parent peak height, as expected.

Consider what happens as the locus of the center of the charge cloud approaches the front surface. This is shown schematically in Figure 6.

There are 4 critical regions in Figure 6:

- (1) The front metal contact layer,
- (2) Interfacial layer where incomplete charge collection will occur,
- (3) A region close to the detector front surface where incomplete charge collection is possible,
- (4) The detector region away from the front surface where all charge will be absorbed, assuming no losses at the side or rear walls.

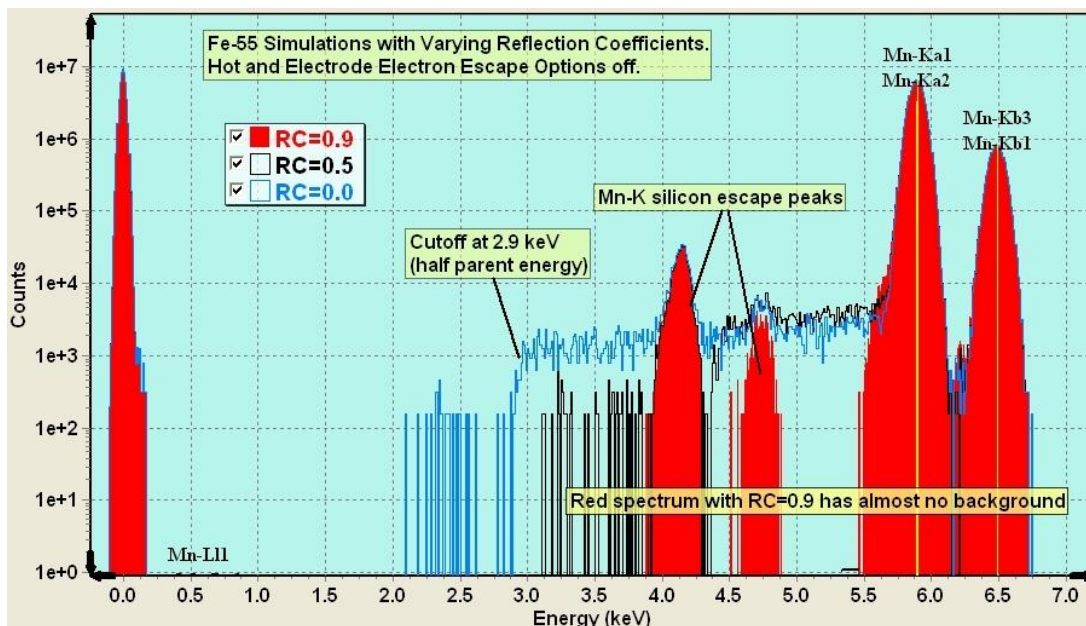


Figure 7. Fe-55 Simulations with Varying Reflection Coefficients.

RESULTS

Figure 8 shows a spectrum that has been modeled with the default parameters in X-Tracker (black line), and compares it with a real Fe-55 source spectrum. The two spectra were normalized in energy, and in intensity by the region around the Mn-K peaks.

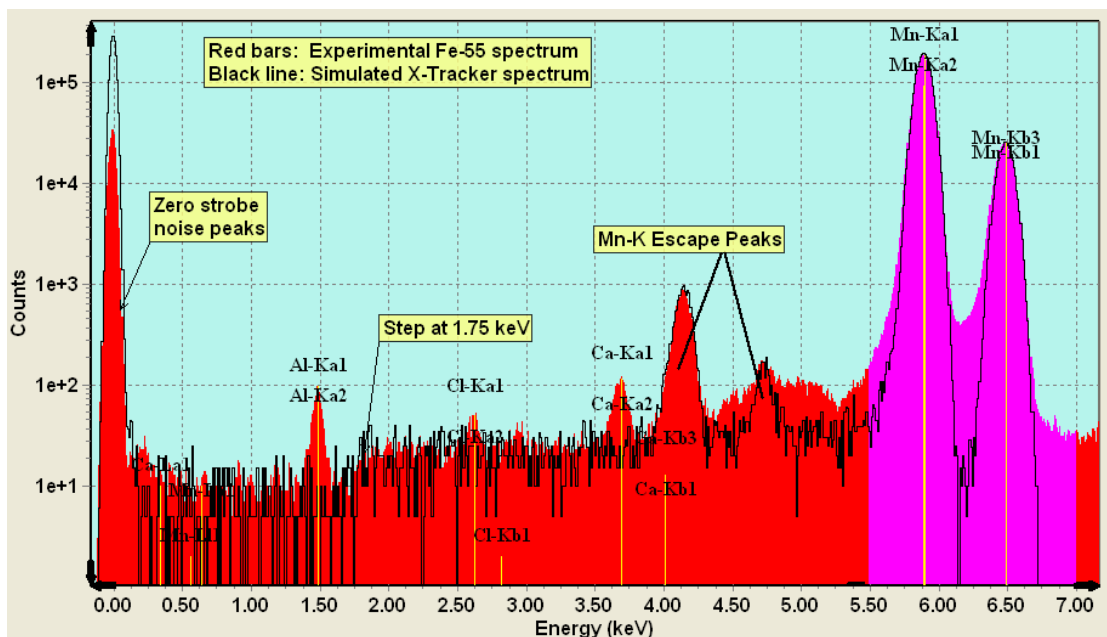


Figure 8. Comparison of Real and Simulated Fe-55 Spectra.

The relative peak heights are well correlated, showing the artificial source file has good starting parameters. Similarly, the escape-peak heights exactly match each other, showing that this part of the simulation is working well. There are several artifact peaks (Al, Cl and Ca) that are from either the source or environment, which we can ignore for now. The overall background shapes

agree very well below the escape peaks, including the step at about 1.75 keV. There is a region around the Mn-K β escape peak that does not agree well, and this is thought to arise from radiative Auger satellite peaks [20]. These peaks are not well defined, and need to be studied further. Although the top 99% of the two main Mn-K peaks fit very well, there is disagreement in the tails (note that Figure 8 is on a log scale). This is mostly on the low-energy sides, and the source for this discrepancy is not yet known, but could be a variation in the field strength and hence collection efficiency, or incorrect values for the mobilities or lifetimes. Another possibility is scattering or other effect occurring either within the source, or in the experimental setup, that causes the tailing. Again, this will be the subject of future investigations.

CONCLUSIONS

We have successfully modeled the response of Si(Li) detectors below 10 keV. Compared with experimental Fe-55 spectra we have demonstrated good agreement with many of the features seen in these spectra. A reflection coefficient feature has been included in the Monte-Carlo simulation that allows us to simulate background or tailing artifacts that are seen in spectra, or even low-energy peak shifts. It has been possible to demonstrate other internal artifacts in X-ray spectra that come from passivation layers and both the front and rear contacts. In the future we will be refining the model to include radiative Auger peaks in the source as well as trying to improve the poor tail fits observed with Fe-55 and other sources, including those at higher energies. We also plan to model detectors with more complex geometries to see if this changes some of the observed response functions.

REFERENCES

- [1] Doster, J.M.; Gardner, R.P., *X-Ray Spectrometry*, **1982**, *11*, 173.
- [2] He, T.; Gardner, R.P.; and Verghese, K., *Nucl. Instr. Methods*, **1990**, *A299*, 354.
- [3] van Dyck, P.; Török, S.; van Grieken, R., *X-Ray Spectrometry*, **1986**, *15*, 231.
- [4] Janssens, K.; Vincze, L.; van Espen, P.; Adams, F., *X-Ray Spectrometry*, **1993**, *22*, 234.
- [5] Mantler, M., *Adv. X-ray Analysis*, **1997**, *41*, 753.
- [6] Campbell, J.L.; McDonald, L.; Hopmann, T.; Papp, T., *X-Ray Spectrometry*, **2001**, *30*, 230.
- [7] Eggert, T.; Boslau, O.; Goldstrass, P.; Kemmer, J.; Pahlke, A.; Wiest, F., *paper presented at the 10th European Symposium on Semiconductor Detectors*, **2005**, Wilbad Kreuth, Germany, June 12-16.
- [8] Joy, D.C., *Monte Carlo Modeling for Electron Microscopy and Microanalysis*, Oxford University Press, New York, **1995**.
- [9] Newbury, D.E.; Myklebust, R.L., *Microbeam Analysis*, **1995**, *4*, 165.
- [10] Reimer, L., *Proceedings EMAS Workshop*, **1995**, *4*, 31.
- [11] Bale, G., *Ph.D. Thesis*, Univ. Leicester, UK, **2001**.
- [12] Kalos, M.H.; Whitlock, P.A., *Monte Carlo Methods, Volume 1: Basics*, J. Wiley & Sons, New York, **1986**.
- [13] Shockley, W., *J. Appl. Phys.*, **1938**, *9*, 635.
- [14] Ramo, S., *Proc. IRE*, **1939**, *27*, 584.
- [15] Hecht, K., *Z. Physik*, **1932**, *77*, 235.
- [16] Akutagawa, W.; Zanio, K., *J. Appl. Phys.*, **1969**, *40*, 3838.
- [17] Lowe, B.G., *Nucl. Instr. Methods*, **2000**, *A438*, 247.
- [18] Scholze, F.; Ulm, G., *Nucl. Instr. Methods*, **1994**, *A339*, 339.
- [19] Inskeep, C.; Elad, E.; Sareen, R.A., *IEEE Trans. Nucl. Sci.*, **1974**, *NS-21*, 379.
- [20] van Espen, P.; Nullens, H.; Adams F., *X-Ray Spectrometry*, **1980**, *9*, 126